Anomalous circularly polarized light emission induced by the optical Berry curvature dipole

Yizhou Liu [1,2] and Binghai Yan [2,*]

[1] *School of Physics Science and Engineering, Tongji University, Shanghai 200092, China*

[2] *Department of Condensed Matter Physics, Weizmann Institute of Science, Rehovot 76100, Israel*

(Received 4 July 2023; revised 4 December 2023; accepted 9 January 2024; published 18 January 2024)

The ability to selectively excite light with fixed handedness is crucial for circularly polarized light emission. It is commonly believed that the luminescent material chirality determines the emitted light handedness, regardless of the light emitting direction. In this paper, we propose an anomalous circular polarized light emission (ACPLE) whose handedness actually relies on the emission direction and current direction in electroluminescence. In a solid semiconductor, the ACPLE originates in the band structure topology characterized by the optical Berry curvature dipole. ACPLE exists in inversion-symmetry breaking materials including chiral materials. We exemplify the ACPLE by estimating the high circular polarization ratio in monolayer WS_2. In addition, the ACPLE can be further generalized to magnetic semiconductors in which the optical Berry curvature plays a leading role instead. Our finding reveals intriguing consequences of band topology in light emission and promises optoelectric applications.

DOI: 10.1103/PhysRevB.109.035142

I. INTRODUCTION

Circularly polarized light emission is important for various advanced technologies including 3D display, optoelectrics, information storage, and quantum spintronics [1,2]. The circularly polarized light can be generated through optical fibers composed by a linear polarizer followed by a quarter-wave plate or circularly polarized light emission (CPLE) processes including photoluminescence and electroluminescence in chiral organic luminophores [3–8] and chiral hybrid organic-inorganic perovskites [9,10]. It is commonly believed that the favored light handedness in CPLE is determined by the material chirality but independent of the emitting direction. Recently, a distinct CPLE was reported in the chiral polymers where the favored light handedness depends on both the emitting direction and polymer chirality [11]. Furthermore, the emission-direction-sensitive CPLE generates giant net polarization ratio of CPLE by orders of magnitude. The anomalous CPLE (ACPLE) was interpreted by the orbital-momentum locking, a topological nature of the chiral molecule electronic structure [11,12].

Compared to chiral organic polymers, we are inspired to explore the ACPLE in crystalline solids where the band structure topology [13–16] can play a significant role. For example, the Berry curvature and Berry connection [17] are extensively considered in the content of light absorbance and the resultant photocurrent, such as the photogalvanic effects [18–23], nonlinear anomalous Hall effect [24–27], and the valley Hall effect [28,29].

In solids, giant CPLE was indeed observed in inversion-breaking semiconductors WSe_2 [30] and WS_2 [31] monolayers, where emitted light handedness is switchable by reversing the current flow. It was rationalized by the valley polarization and asymmetric band structures of electrons and holes. Additionally, a magnetization switched CPLE was also reported in a magnetic insulator CrI_3 [32], which was interpreted by local molecular orbital transitions of Cr^{3+} cations. From the theoretical aspect, the electronic wavefunctions and topology should play an essential role there but remain largely unexplored, although the band dispersion (e.g., band shift, and triangular warping etc. [33]) was recently discussed in this context.

In this paper, we formulate the ACPLE that exists in inversion-breaking solids (including chiral solids) by the optical Berry curvature dipole. Different from the ordinary CPLE, the favored light handedness depends both on the direction of applied current and the light-emitting direction. Here, ACPLE can be regarded as a reverse process of the circular photogalvanic effect where CP light irradiation generates a dc signal [19]. We first demonstrate the ACPLE in the strained WS_2 monolayer. The CPLE in WS_2 shows handedness switching by the direction of applied strain, current flow, and emitting direction. In addition, the ACPLE can also appear in magnetic solids, which originate in the optical Berry curvature. Our theory rationalizes the current direction or magnetization-switchable light handedness in previous experiments based on WS_2 or CrI_3. Our predictions can be further verified by detecting the emission-direction dependent handedness in present devices. The ACPLE promises applications in exotic light-emitting diodes and ultrafast optoelectronic information applications.

II. THEORY OF ACPLE

The emission rate of left- (L) and right- (R) handed circularly polarized (CP) light is determined by

$$I_{L/R} = \frac{2\pi}{\hbar} \sum_{c,v,\boldsymbol{k}} |\langle v\boldsymbol{k}|H'|c\boldsymbol{k}\rangle|^2 f_{c\boldsymbol{k}}(1-f_{v\boldsymbol{k}})\delta(\varepsilon_{c\boldsymbol{k}}-\varepsilon_{v\boldsymbol{k}}-\hbar\omega), \quad (1)$$

*binghai.yan@weizmann.ac.il

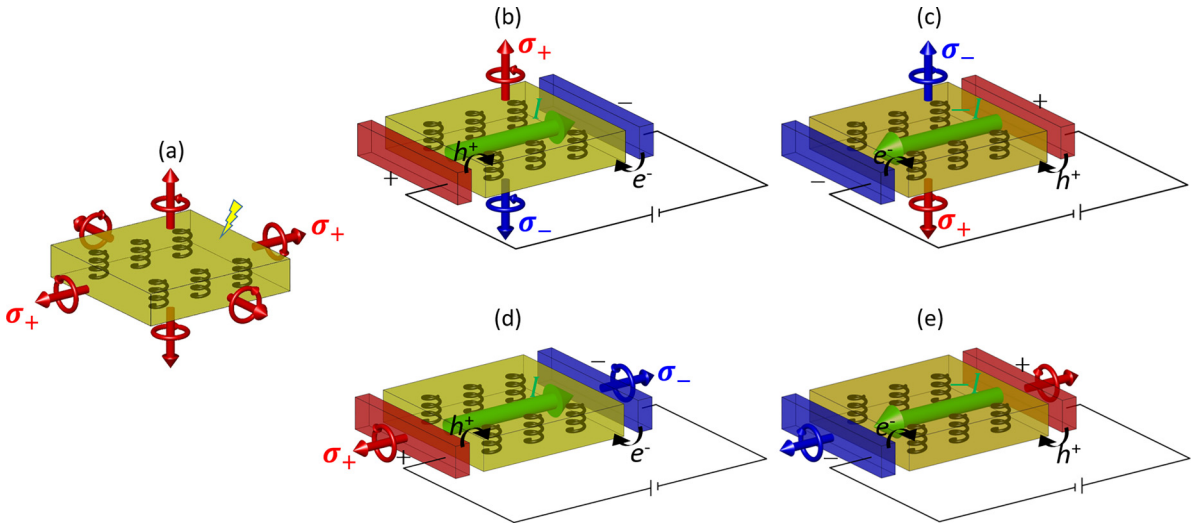

FIG. 1. Schematics of the (a) ordinary CPLE and (b)–(e) ACPLE, respectively. (a) Ordinary CPLE in chiral materials. The favored light handedness depends solely on the chirality of the luminescent material but independent of the emitting direction. [(b)–(e)] The ACPLE induced by finite current in chiral or inversion-symmetry-breaking achiral materials sandwiched by PN junctions. The favored light handedness depends on the emitting direction and also reverses with the direction of current I. For chiral materials the direction of ACPLE can be either parallel or perpendicular to the direction of current [(b)–(e)], but for inversion-symmetry-breaking achiral materials, the ACPLE can be only perpendicular to the current [(b),(c)].

where $|c\boldsymbol{k}\rangle$ ($|v\boldsymbol{k}\rangle$) refers to the Bloch state of conduction (valence) band, $\varepsilon_{c\boldsymbol{k}}$ ($\varepsilon_{v\boldsymbol{k}}$) is the conduction (valence) band energy, $f_{c\boldsymbol{k}}$ is the electron occupation probability in the conduction band and $1-f_{v\boldsymbol{k}}$ refers to the hole occupation in the valence band, and $H' = -e\boldsymbol{E}\cdot\boldsymbol{r} - \boldsymbol{m}\cdot\boldsymbol{B}$ is the light-matter interaction Hamiltonian with $e\boldsymbol{r}$ and $\boldsymbol{m}$ being the electric and magnetic moments, respectively, $\boldsymbol{E}$ and $\boldsymbol{B}$ being the electric and magnetic fields of light, respectively, and $\hbar\omega$ is the photon energy. For CP light with wave vector $\boldsymbol{q}$, the electric and magnetic fields are $\boldsymbol{E} = \frac{E_0}{\sqrt{2}}(\hat{\boldsymbol{e}}_1 \pm i\hat{\boldsymbol{e}}_2)$ and $\boldsymbol{B} = \frac{1}{c_0}\hat{\boldsymbol{q}}\times\boldsymbol{E}$ with $\hat{\boldsymbol{e}}_2$ and $\hat{\boldsymbol{e}}_2$ being the two unit vectors perpendicular to $\boldsymbol{q}$, c_0 is speed of light, and $\hat{\boldsymbol{q}} = \boldsymbol{q}/|\boldsymbol{q}|$ is the unit vector of $\boldsymbol{q}$.

The difference of generated CP light emission can be calculated as

$$I_L - I_R = -\frac{2\pi e^2}{\hbar}|E_0|^2\sum_{c,v,\boldsymbol{k}} f_{c\boldsymbol{k}}(1-f_{v\boldsymbol{k}})\delta(\varepsilon_{c\boldsymbol{k}}-\varepsilon_{v\boldsymbol{k}}-\hbar\omega) \times\left[\frac{2}{ec_0}\mathrm{Im}\left(r_1^{vc}m_1^{cv}+r_2^{vc}m_2^{cv}\right)+\boldsymbol{\Omega}^{vc}\cdot\hat{\boldsymbol{q}}+O(m^2)\right], \tag{2}$$

where $r_i^{vc} = \langle c\boldsymbol{k}|\boldsymbol{r}\cdot\hat{\boldsymbol{e}}_i|v\boldsymbol{k}\rangle$ and $m_i^{cv} = \langle c\boldsymbol{k}|\boldsymbol{m}\cdot\hat{\boldsymbol{e}}_i|v\boldsymbol{k}\rangle$ $(i=1,2)$ refer to the electric and magnetic transition dipoles within the polarization plane of $\hat{\boldsymbol{e}}_1$ and $\hat{\boldsymbol{e}}_2$. $\boldsymbol{\Omega}^{vc} = -i\boldsymbol{r}^{vc}\times\boldsymbol{r}^{cv}$ is the interband Berry curvature [34,35] whose expression is given by

$$\Omega_a^{vc} = -i\epsilon_{abd}r_b^{vc}r_d^{cv} = -\hbar^2\epsilon_{abd}\mathrm{Im}\frac{\langle v\boldsymbol{k}|v_b|c\boldsymbol{k}\rangle\langle c\boldsymbol{k}|v_d|v\boldsymbol{k}\rangle}{(\varepsilon_{c\boldsymbol{k}}-\varepsilon_{v\boldsymbol{k}})^2}, \tag{3}$$

where $a,b,d = x,y,z$ refer to Cartesian coordinates, ϵ_{abd} refers to the rank-3 antisymmetric Levi-Civita tensor, and v_b, v_d refer to the velocity operator. The first term on the second line of Eq. (2) gives rise to the ordinary CPLE or natural circular dichroism, which has been extensively investigated in nonmagnetic chiral molecules and polymers [5,36] as shown in Fig. 1(a).

The second term in Eq. (2) ($\boldsymbol{\Omega}^{vc}\cdot\hat{\boldsymbol{q}}$) gives rise to the ACPLE. Recently, the ACPLE in chiral organic molecules is reported and the interband Berry curvature $\boldsymbol{\Omega}^{vc}$ was interpreted as orbital angular momentum because $i\boldsymbol{r}^{vc}\times\boldsymbol{r}^{cv} = \frac{1}{m_e\omega}\boldsymbol{r}^{vc}\times\boldsymbol{p}^{cv}$, where $\boldsymbol{p} = m_e\boldsymbol{v}$ refers to the momentum operator [11]. This anomalous term is usually neglected before because the total Berry curvature vanishes in nonmagnetic materials such as organic molecules and polymers. It is not surprising that this term becomes significant in magnetic materials. Here, the magnetic order determines the sign of $\boldsymbol{\Omega}^{vc}$ and thereafter the sign of CPLE polarization. Furthermore, $\boldsymbol{\Omega}^{vc}\cdot\hat{\boldsymbol{q}}$ clearly indicates the emission-direction ($\hat{\boldsymbol{q}}$) dependence of CPLE, which was not aware of before. Because the nonequilibrium current flow breaks time-reversal symmetry (TRS) even in nonmagnetic materials, the ACPLE term is also significant in CPLE.

For a nonmagnetic system with TRS, the Berry curvature satisfies $\boldsymbol{\Omega}^{vc}(\boldsymbol{k}) = -\boldsymbol{\Omega}^{vc}(-\boldsymbol{k})$, which makes the anomalous term cancel with each other between $\boldsymbol{k}$ and $-\boldsymbol{k}$ at thermodynamic equilibrium. Therefore there are two cases the anomalous term can take effect: (i) The TRS is broken by spontaneous magnetization (e.g., CrI_3 monolayer); (ii) the system is in nonequilibrium state with the occupation probability satisfying $f_{c\boldsymbol{k}} \neq f_{c-\boldsymbol{k}}$ and $f_{v\boldsymbol{k}} \neq f_{v-\boldsymbol{k}}$ driving by an external electrical current, i.e., the ACPLE as shown in Figs. 1(b) and 1(c). Switching the current direction reverses the induced polarization. Particularly the anomalous term explicitly depends on the light-emitting direction $\hat{\boldsymbol{q}}$ resulting in the direction-dependent CPLE signals.

Optical Berry curvature dipole. In nonmagnetic materials, the system is driven out of thermal equilibrium by an external electrical current. The nonequilibrium distribution

functions $f_{c\boldsymbol{k}}$ and $f_{v\boldsymbol{k}}$ can be determined by the Boltzmann equation under relaxation time approximation,

$$f_{\alpha\boldsymbol{k}} = f^0_{\alpha\boldsymbol{k}} + \tau \frac{e}{\hbar}\boldsymbol{\mathcal{E}} \cdot \boldsymbol{\nabla}_{\boldsymbol{k}} f^0_{\alpha\boldsymbol{k}} + O(\tau^2), \tag{4}$$

where $\alpha = c, v$ and $f^0_{\alpha\boldsymbol{k}} = [e^{(\varepsilon_{\alpha\boldsymbol{k}}-\mu)/k_BT}+1]^{-1}$ refers to the equilibrium Fermi distribution function, τ is the relaxation time, and $\boldsymbol{\mathcal{E}}$ is the external electrical field. Substitute Eq. (4) into Eq. (2), the ACPLE [second term of Eq. (2)] can be calculated as

$$\begin{aligned} I_L - I_R &= \frac{2\pi e^2}{\hbar}|E_0|^2 f_B(\hbar\omega) j_a D_{ab}(\hbar\omega)\hat{q}_b + O(\tau^2), \\ D_{ab}(\hbar\omega) &= \frac{e\tau}{\sigma_{aa}} \sum_{c,v,\boldsymbol{k}} \left(f^0_{v\boldsymbol{k}} - f^0_{c\boldsymbol{k}}\right)\partial_{k_a}\Omega^{vc}_b(\boldsymbol{k},\omega), \end{aligned} \tag{5}$$

where $j_a = \sigma_{aa}\mathcal{E}_a$ is the electrical current density, and $\sigma_{aa} = e^2\tau\sum_{c,v,\boldsymbol{k}}[(v^a_{v\boldsymbol{k}})^2(-\frac{\partial f^0_{v\boldsymbol{k}}}{\partial\varepsilon_{v\boldsymbol{k}}}) + (v^a_{c\boldsymbol{k}})^2(-\frac{\partial f^0_{c\boldsymbol{k}}}{\partial\varepsilon_{c\boldsymbol{k}}})]$ is the electrical conductivity. The identity $f^0_{c\boldsymbol{k}}(1-f^0_{v\boldsymbol{k}}) = f_B(\varepsilon_{c\boldsymbol{k}}-\varepsilon_{v\boldsymbol{k}})(f^0_{v\boldsymbol{k}} - f^0_{c\boldsymbol{k}})$ has been used in the derivation. Here $f_B(\hbar\omega) = (e^{\hbar\omega/k_BT}-1)^{-1}$ is the Bose distribution function. The optical Berry curvature (OBC) refers to Berry curvature at the optical transition energy $\hbar\omega$,

$$\Omega^{vc}_b(\boldsymbol{k},\omega) = \hat{\boldsymbol{e}}_b \cdot \boldsymbol{\Omega}^{vc}(\boldsymbol{k})\delta(\varepsilon_{c\boldsymbol{k}} - \varepsilon_{v\boldsymbol{k}} - \hbar\omega), \tag{6}$$

which represent the bth component. The $D_{ab}(\hbar\omega)$, as expressed on the last line of Eq. (5), represents the sum of the optical Berry curvature dipole (OBCD). In contrast to the ordinary Berry curvature dipole [24], the OBCD is not a Fermi-surface property as it involves empty conduction bands. It is a rank-2 pseudotensor, i.e., it is even under TRS but odd under inversion, so that the ACPLE in Eq. (5) can only occur in inversion-symmetry-breaking materials including chiral materials. In addition to the material-specific OBCD, the ACPLE is also linear to the electrical current $\boldsymbol{j}$, which rationalize previous experimental results about electrical switchable ACPLE [30].

What was uncovered in previous experiments is that the ACPLE also depends on the emission direction $\hat{\boldsymbol{q}}$. In optoelectronic literature, a dimensionless dissymmetry factor $g = (I_L - I_R)/\frac{1}{2}(I_L + I_R)$ is often used to describe the circular polarization ratio. The dissymmetry factor for the ACPLE is

$$g_{\mathrm{EL}} = \frac{2 j_a D_{ab}\hat{q}_b}{I_0} + O(\tau^2), \tag{7}$$

where $I_0 = \sum_{c,v,\boldsymbol{k}}(|r^{vc}_1|^2 + |r^{vc}_2|^2)\delta(\varepsilon_{c\boldsymbol{k}} - \varepsilon_{v\boldsymbol{k}} - \hbar\omega)$ is the ordinary absorption magnitude. According to Eq. (7), the dissymmetry factor can be enhanced by increasing electrical current $\boldsymbol{j}$ besides optimizing OBCD.

In the context of the nonlinear anomalous Hall effect [24], the intraband Berry curvature dipole was discussed only the off-diagonal components contribute to nonlinear Hall conductivity. In contrast, the ACPLE exists for both $a \neq b$ and $a = b$ in Eq. (5). If $a = b$, the material should be chiral because either inversion symmetry or mirror symmetry forces D_{aa} to vanish. If $a \neq b$, the material only requires to break the inversion symmetry, which also applies for chiral materials. In the device, $a \neq b$ ($a = b$) means that light emission direction $\hat{q}_b$ is normal [see Figs. 1(b) and 1(c)] {parallel [see Figs. 1(d) and 1(e)]}to the current flow.

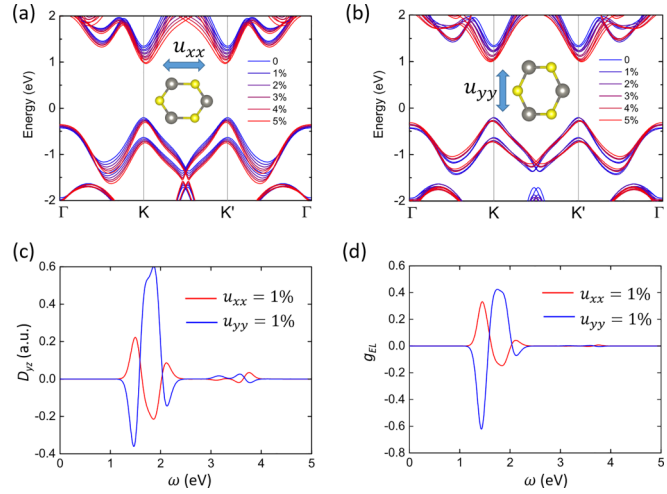

FIG. 2. ACPLE in strained WS_2 monolayer. [(a),(b)] Evolution of band structures of WS_2 monolayers under unidirectional strain u_{xx} and u_{yy}, respectively. [(c),(d)] Calculated D_{yz} and g_{EL} for different strains at $T = 300$ K. Under uniaxial strain u_{xx} and u_{yy}, $D_{xz}(\omega)$ vanishes because of the combined mirror-time-reversal symmetry $M_y\mathcal{T}$. The current density $j_y = 10^{-6}$ A/m has been chosen in the calculation of g_{EL}.

III. ACPLE IN INVERSION ASYMMETRIC MATERIALS

Among the various inversion asymmetric materials found so far, the transition metal dichalcogenides (TMDs) are of particular interest because of the low-energy Dirac physics at Brillouin zone corners K and K', which exhibit valley-contrasting CP excitations processes. Zhang *et al.* first demonstrated the electrically switchable CPLE in a WSe_2 monolayer transistor [30] and this effect was attributed to the triangular warping effect of the band structure [30,33]. Recently Pu *et. al.* have experimentally demonstrated the room-temperature chiral light-emitting diode in strained WS_2 monolayer [31]. In the following we illustrate the role of OBCD in the ACPLE of strained WS_2 monolayer.

The crystal structure of unstrained WS_2 monolayer has a threefold rotation symmetry C_{3z}, under which the OBCD D_{ab} ($a = x, y$, and $b = z$) vanishes for any ω. Therefore any finite Berry dipole requires the breaking of C_{3z}, which can be realized by an externally applied uniaxial strain field u_{xx} and u_{yy}. Figure 2 shows the calculated band structure, OBCD, and g_{EL} of WS_2 monolayer under different strain conditions based on first-principles methods (see Methods section for details). The calculated OBCD and g_{EL} vanish for the unstrained case but become nonzero with finite u_{xx} or u_{yy}, which is consistent with the symmetry analysis.

On the other hand the strain-induced OBCD and g_{EL} are of opposite sign between u_{xx} and u_{yy} as shown in Figs. 2(c) and 2(d), which enables strain engineering of ACPLE in WS_2 monolayer. According to the semiclassical theory, the applied strain can induce an effective gauge potential [37,38]

$$\boldsymbol{A}^{\mathrm{eff}} = \tau_z \frac{\beta}{a_0}(-2u_{xy}, u_{xx} - u_{yy}), \tag{8}$$

where a_0 is the lattice constant, β is a parameter proportional to the electron-phonon coupling strength, and u_{ab} ($a, b = x, y$) refers to the applied external strain tensor. $\tau_z = \pm 1$ is the

valley index indicating K and K' valleys, respectively, reflecting the fact that the induced effective gauge potential are of opposite signs between two valleys, which is a manifestation of the global TRS. According to Eq. (8) the gauge potentials induced by different uniaxial strains u_{xx} and u_{yy} are of the opposite signs, which moves the conduction and valence bands along opposite directions as is shown in Figs. 2(a) and 2(b). As a result the induced OBCD and $g_{\rm EL}$ are of opposite sign for nonzero u_{xx} and u_{yy} as is shown in Figs. 2(c) and 2(d). The calculated value of $g_{\rm EL}$ depends on magnitude of the applied current $\boldsymbol{j}$. Under the applied current density $j = 10^{-6}$ A/m the calculated maximum $g_{\rm EL}$ is about 0.62 (polarization rate 31%) at around 1.43 eV, which is comparable to the experimental value of polarization rate between 9% and 24% [31]. The $g_{\rm EL}$ can be further enhanced by using larger electrical current according to Eq. (7). However, it should be noted that $g_{\rm EL}$ cannot become infinitely large with increasing j because it is bounded as $|g_{\rm EL}| \leqslant 2$ by its definition. This is because the relaxation time approximation in Eq. (4) is valid only under moderate $|\boldsymbol{\mathcal{E}}|$ and τ, which can be justified by the fact that the values of occupations $f_{\alpha\boldsymbol{k}}$ and $f^0_{\alpha\boldsymbol{k}}$ must be bounded by $0 \leqslant f_{\alpha\boldsymbol{k}}, f^0_{\alpha\boldsymbol{k}} \leqslant 1$ so that $\tau\frac{e}{\hbar}|\boldsymbol{\mathcal{E}}\cdot\boldsymbol{\nabla}_{\boldsymbol{k}} f^0_{\alpha\boldsymbol{k}}| = |f_{\alpha\boldsymbol{k}} - f^0_{\alpha\boldsymbol{k}}| \leqslant 1$. For significantly large values of $|\boldsymbol{\mathcal{E}}|$ and τ (so large current density j), the higher-order terms in $O(\tau^2)$ and the achiral magnetic dipole contributions $O(m^2)$ of Eq. (2) must be included [39]. The ACPLE in WS_2 monolayer exhibit rich switchable properties controlled by the direction of applied electrical current, strain, and emitting directions, which is favorable for future optoelectronic device applications.

IV. ACPLE IN MAGNETIC MATERIALS

CrI_3 is a van der Waals magnetic material with (anti-) ferromagnetic (interlayer) intralayer coupling [40,41]. Its monolayer exhibit in-plane ferromagnetism, which breaks the TRS. The crystal structure has inversion symmetry, which prohibit the ordinary term in Eq. (2) so that only the anomalous term contributes to the CPLE.

We calculate the ACPLE in the ferromagnetic CrI_3 monolayer. The ACPLE in CrI_3 is determined by the OBC $\Omega(\boldsymbol{k},\omega)$, which is the product of interband Berry curvature $\Omega^{vc}_{\boldsymbol{k}}$ and the joint density of states (JDOS) $g^{cv}_j(\boldsymbol{k},\omega) = \delta(\varepsilon_{c\boldsymbol{k}} - \varepsilon_{v\boldsymbol{k}} - \hbar\omega)$. Figure 3(a) shows the electronic band structure of CrI_3 monolayer along high-symmetry lines (HSLs) with a direct band gap of 0.85 eV at Γ point. Derived from the band structure and Bloch wave functions along the HSLs, we plotted the optical excitation energy spectrum $\hbar\omega = \varepsilon_{c\boldsymbol{k}} - \varepsilon_{v\boldsymbol{k}}$ together with $\boldsymbol{k}$-resolved optical Berry curvature $\Omega(\boldsymbol{k},\omega) = \sum_{c,v}\Omega^{vc}_z(\boldsymbol{k},\omega)$ along high-symmetry lines (HSLs) in Fig. 3(b). The interband Berry curvature generally decreases with increasing ω because $\Omega^{cv}_{\boldsymbol{k}} \propto \frac{1}{(\varepsilon_{c\boldsymbol{k}}-\varepsilon_{v\boldsymbol{k}})^2} \propto \frac{1}{\omega^2}$; however, the JDOS $g^{cv}_j(\omega)$ generally increase with ω because of the increasing number of channels. As a result, there exist a maximum value of the optical Berry curvature $\Omega(\omega)$ as function of ω as is shown in the red line of Fig. 3(c). We also calculated the dissymmetry factor for the ACPLE

$$g_{PL} = 2\times\frac{I_L - I_R}{I_L + I_R} = \frac{2\Omega(\omega)}{I_0} \tag{9}$$

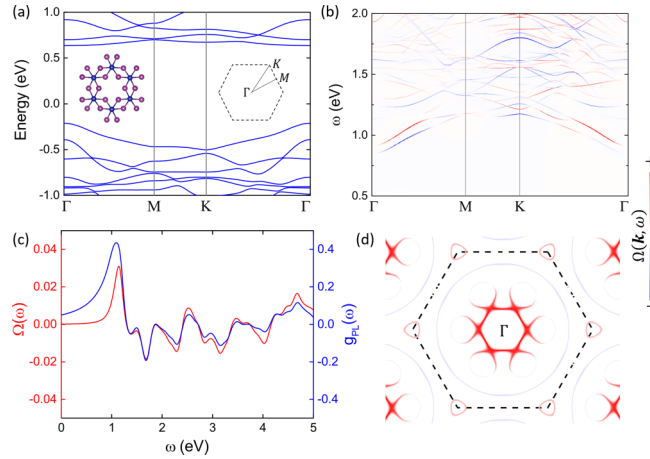

FIG. 3. Anomalous CP PL in magnetic CrI_3 monolayer. (a) Band structure of CrI_3 monolayer whose crystal structure and Brillouin zone are shown in the insets. (b) Distribution of optical Berry curvature dipole $\Omega(\boldsymbol{k},\omega)$ along hight-symmetry lines. (c) Integrated total optical Berry curvature $\Omega(\omega) = \sum_{\boldsymbol{k}}\Omega(\boldsymbol{k},\omega) = \sum_{c,v,\boldsymbol{k}}\Omega^{vc}_{\boldsymbol{k}}\delta(\varepsilon_{c\boldsymbol{k}} - \varepsilon_{v\boldsymbol{k}} - \hbar\omega)$ and dissymmetry factor $g_{PL} = 2(I_L - I_R)/(I_L + I_R)$ as functions of ω. The peak value of $g_{PL} \sim 0.42$ at $\omega = 1.14$ is comparable to the experimental value of maximum g value of around 1 at $\omega = 1.15$ eV [32]. (d) Momentum resolved optical Berry curvature distribution $\Omega(\boldsymbol{k},\omega)$ at the peak value of $\omega = 1.14$ eV.

as shown in the blue line of Fig. 3(c), where $\Omega(\omega) = \sum_{c,v,\boldsymbol{k}}\Omega^{vc}_z(\boldsymbol{k},\omega)$ refers to the total OBC. It should be noted that the dissymmetry factor g_{PL} in CrI_3 is determined only by band structure properties in contrast to the $g_{\rm EL}$ in WS_2, which also depends on external electrical current j. Figure 3(d) shows the $\boldsymbol{k}$-resolved distribution of the optical Berry curvature $\Omega(\boldsymbol{k},\omega)$ at the peak value $\omega = 1.14$ eV of the curve of optical Berry curvature $\Omega(\omega)$, which indicates the most prominent contribution from the highest valence band and the second lowest conduction band. The calculated maximum g_{PL} of CrI_3 monolayer approaches about 0.42 at $\omega \approx 1.14$ eV, which matches the order of magnitude with the experimental $g \approx 1$ at $\omega = 1.15$ eV [32]. Here, reversing the magnetization lead to opposite $\Omega(\omega)$ and thus opposite g_{PL}.

V. DISCUSSION

Because of the intimate relation between Berry curvature (dipole) and linear (nonlinear) anomalous Hall effect (AHE) [17,24,42], the ACPLE satisfies a sum rule,

$$\int_0^{+\infty} d\omega\,\frac{I_L - I_R}{f_B(\hbar\omega)} = \frac{2\pi}{\hbar}|E_0|^2\sigma^{\rm AH} = \mathcal{C}\frac{e^2}{\hbar^2}I_0, \tag{10}$$

where $\sigma^{\rm AH} = \mathcal{C}e^2/h$ refers to the quantized anomalous Hall conductivity perpendicular $\hat{\boldsymbol{q}}$, $\mathcal{C}$ is the Chern number, and $I_0 = |E_0|^2$ is the intensity of light. For 2D semiconductors/insulators, the linear AHE conductivity is quantized in multiples of e^2/h, and Eq. (10) shows that the integrated ACPLE is quantized in unit of $(e^2/\hbar^2)I_0$. Thus the integrated ACPLE spectrum give rise to topologically

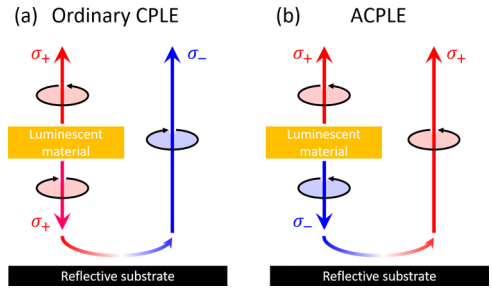

FIG. 4. Comparison between (a) ordinary CPLE and (b) ACPLE in the presence of reflective substrates. The net polarization of ordinary CPL is suppressed while it is enhanced for the ACPLE.

quantized signals, which awaits for future experimental verification.

The emission-direction dependence of ACPLE is a characteristic feature compared to the ordinary CPLE. In literature, CPLE is usually studied with the exciton-coupling model [43,44], which cannot rationalize the current-direction and emission-direction dependence of ACPLE.

The emission-direction has a significant impact to enhance the polarization of a LED device. Figure 4 shows the geometry of back-reflective LED. For the ordinary CPLE, the emitted CP light is of the same handedness for both directions. The handedness changed after back reflection [Fig. 4(a)]. Therefore, the net polarization diminishes when both light beams mix together. On the other hand, for the ACPLE, the handedness of the CP light for both directions are opposite. After reflection, both light beams exhibit the same handedness, avoiding the cancellation of polarization [Fig. 4(b)]. Furthermore, the current-direction dependence enables high-speed switching of the light handedness by electric control, which is essential for future optical quantum technology.

VI. SUMMARY

In summary, we proposed the quantum theory of anomalous circular polarized light emission based on the optical Berry curvature and Berry curvature dipole. Our calculations on WS_2 and CrI_3 monolayers are consistent with recent experimental results. We propose that experiments can further detect the emission-direction dependence of the light handedness. Our findings deepen the understanding of band topology induced exotic optical phenomena and promise technology applications for high-speed, handedness-tunable optoelectrics.

VII. METHODS

First-principles calculations. Our first-principles calculations are based on density functional theories as implemented in Vienna *ab initio* Simulation Packages (VASP) [45]. The generalized gradient approximation of Perdew-Burke-Ernzerhof type [46] has been used for the exchange-correlation functionals. A 15×15 k mesh and cut-off energy 280 eV are used for self-consistent ground-state energy calculation. The tight-binding Hamiltonians of CrI_3 and WS_2 monolayers are constructed using the Wannier90 code [47–49]. For WS_2, the localized Wannier orbitals are constructed based on the $5d$ orbitals of W atom and $3s$, $3p$ orbitals of S atom; for CrI_3, the $3d$ orbitals of Cr atom and $5p$ orbitals of I atom are used.

ACKNOWLEDGMENTS

We thank Daniel Kaplan and Hengxin Tan for helpful discussions. B.Y. acknowledges the financial support by the European Research Council (ERC Consolidator Grant "NonlinearTopo", No. 815869) and the Minerva foundation with funding from the Federal German Ministry for Education and Research. Y.L. is sponsored by the Shanghai Pujiang Program (Grant No. 23PJ1413000).

[1] D.-W. Zhang, M. Li, and C.-F. Chen, Recent advances in circularly polarized electroluminescence based on organic light-emitting diodes, Chem. Soc. Rev. **49**, 1331 (2020).

[2] J. Han, S. Guo, H. Lu, S. Liu, Q. Zhao, and W. Huang, Recent progress on circularly polarized luminescent materials for organic optoelectronic devices, Adv. Opt. Mater. **6**, 1800538 (2018).

[3] J. P. Riehl and F. S. Richardson, Circularly polarized luminescence spectroscopy, Chem. Rev. **86**, 1 (1986).

[4] E. M. Sánchez-Carnerero, A. R. Agarrabeitia, F. Moreno, B. L. Maroto, G. Muller, M. J. Ortiz, and S. de la Moya, Circularly polarized luminescence from simple organic molecules, Chem. Eur. J. **21**, 13488 (2015).

[5] G. Longhi, E. Castiglioni, J. Koshoubu, G. Mazzeo, and S. Abbate, Circularly polarized luminescence: A review of experimental and theoretical aspects, Chirality **28**, 696 (2016).

[6] Y. Sang, J. Han, T. Zhao, P. Duan, and M. Liu, Circularly polarized luminescence in nanoassemblies: Generation, amplification, and application, Adv. Mater. **32**, 1900110 (2020).

[7] Y. Deng, M. Wang, Y. Zhuang, S. Liu, W. Huang, and Q. Zhao, Circularly polarized luminescence from organic micro-/nano-structures, Light: Sci. Appl. **10**, 76 (2021).

[8] J. Crassous, M. J. Fuchter, D. E. Freedman, N. A. Kotov, J. Moon, M. C. Beard, and S. Feldmann, Materials for chiral light control, Nat. Rev. Mater. **8**, 365 (2023).

[9] Y.-H. Kim, Y. Zhai, H. Lu, X. Pan, C. Xiao, E. A. Gaulding, S. P. Harvey, J. J. Berry, Z. V. Vardeny, J. M. Luther, and M. C. Beard, Chiral-induced spin selectivity enables a room-temperature spin light-emitting diode, Science **371**, 1129 (2021).

[10] G. Long, R. Sabatini, M. I. Saidaminov, G. Lakhwani, A. Rasmita, X. Liu, E. H. Sargent, and W. Gao, Chiral-perovskite optoelectronics, Nat. Rev. Mater. **5**, 423 (2020).

[11] L. Wan, Y. Liu, M. J. Fuchter, and B. Yan, Anomalous circularly polarized light emission in organic light-emitting diodes caused by orbital–momentum locking, Nat. Photonics **17**, 193 (2023).

[12] Y. Liu, J. Xiao, J. Koo, and B. Yan, Chirality-driven topological electronic structure of DNA-like materials, Nat. Mater. **20**, 638 (2021).

[13] M. Z. Hasan and C. L. Kane, Colloquium: Topological insulators, Rev. Mod. Phys. **82**, 3045 (2010).

[14] X.-L. Qi and S.-C. Zhang, Topological insulators and superconductors, Rev. Mod. Phys. **83**, 1057 (2011).

[15] B. Yan and C. Felser, Topological materials: Weyl semimetals, Annu. Rev. Condens. Matter. Phys. **8**, 337 (2017).

[16] N. P. Armitage, E. J. Mele, and A. Vishwanath, Weyl and Dirac semimetals in three-dimensional solids, Rev. Mod. Phys. **90**, 015001 (2018).

[17] D. Xiao, M.-C. Chang, and Q. Niu, Berry phase effects on electronic properties, Rev. Mod. Phys. **82**, 1959 (2010).

[18] R. von Baltz and W. Kraut, Theory of the bulk photovoltaic effect in pure crystals, Phys. Rev. B **23**, 5590 (1981).

[19] J. E. Sipe and A. I. Shkrebtii, Second-order optical response in semiconductors, Phys. Rev. B **61**, 5337 (2000).

[20] P. Hosur, Circular photogalvanic effect on topological insulator surfaces: Berry-curvature-dependent response, Phys. Rev. B **83**, 035309 (2011).

[21] T. Morimoto and N. Nagaosa, Topological nature of nonlinear optical effects in solids, Sci. Adv. **2**, e1501524 (2016).

[22] T. Holder, D. Kaplan, and B. Yan, Consequences of time-reversal-symmetry breaking in the light-matter interaction: Berry curvature, quantum metric, and diabatic motion, Phys. Rev. Res. **2**, 033100 (2020).

[23] F. de Juan, A. G. Grushin, T. Morimoto, and J. E. Moore, Quantized circular photogalvanic effect in Weyl semimetals, Nat. Commun. **8**, 15995 (2017).

[24] I. Sodemann and L. Fu, Quantum nonlinear Hall effect induced by berry curvature dipole in time-reversal invariant materials, Phys. Rev. Lett. **115**, 216806 (2015).

[25] Y. Zhang, Y. Sun, and B. Yan, Berry curvature dipole in Weyl semimetal materials: An *ab initio* study, Phys. Rev. B **97**, 041101(R) (2018).

[26] Q. Ma, S.-Y. Xu, C.-K. Chan, C.-L. Zhang, G. Chang, Y. Lin, W. Xie, T. Palacios, H. Lin, S. Jia *et al.*, Direct optical detection of Weyl fermion chirality in a topological semimetal, Nat. Phys. **13**, 842 (2017).

[27] K. Kang, T. Li, E. Sohn, J. Shan, and K. F. Mak, Nonlinear anomalous Hall effect in few-layer WTe_2, Nat. Mater. **18**, 324 (2019).

[28] D. Xiao, W. Yao, and Q. Niu, Valley-contrasting physics in graphene: Magnetic moment and topological transport, Phys. Rev. Lett. **99**, 236809 (2007).

[29] W. Yao, D. Xiao, and Q. Niu, Valley-dependent optoelectronics from inversion symmetry breaking, Phys. Rev. B **77**, 235406 (2008).

[30] Y. J. Zhang, T. Oka, R. Suzuki, J. T. Ye, and Y. Iwasa, Electrically switchable chiral light-emitting transistor, Science **344**, 725 (2014).

[31] J. Pu, W. Zhang, H. Matsuoka, Y. Kobayashi, Y. Takaguchi, Y. Miyata, K. Matsuda, Y. Miyauchi, and T. Takenobu, Room-temperature chiral light-emitting diode based on strained monolayer semiconductors, Adv. Mater. **33**, 2100601 (2021).

[32] K. L. Seyler, D. Zhong, D. R. Klein, S. Gao, X. Zhang, B. Huang, E. Navarro-Moratalla, L. Yang, D. H. Cobden, M. A. McGuire *et al.*, Ligand-field helical luminescence in a 2D ferromagnetic insulator, Nat. Phys. **14**, 277 (2018).

[33] S. Wang, M. S. Ukhtary, and R. Saito, Strain effect on circularly polarized electroluminescence in transition metal dichalcogenides, Phys. Rev. Res. **2**, 033340 (2020).

[34] S.-Y. Xu, Q. Ma, H. Shen, V. Fatemi, S. Wu, T.-R. Chang, G. Chang, A. M. M. Valdivia, C.-K. Chan, Q. D. Gibson *et al.*, Electrically switchable Berry curvature dipole in the monolayer topological insulator WTe_2, Nat. Phys. **14**, 900 (2018).

[35] M. S. Okyay, S. A. Sato, K. W. Kim, B. Yan, H. Jin, and N. Park, Second harmonic Hall responses of insulators as a probe of Berry curvature dipole, Commun. Phys. **5**, 303 (2022).

[36] N. Berova, K. Nakanishi, and R. W. Woody, *Circular Dichroism: Principles and Applications* (John Wiley & Sons, Hoboken, NJ, 2000).

[37] F. Guinea, M. Katsnelson, and A. Geim, Energy gaps and a zero-field quantum Hall effect in graphene by strain engineering, Nat. Phys. **6**, 30 (2010).

[38] M. A. Cazalilla, H. Ochoa, and F. Guinea, Quantum spin Hall effect in two-dimensional crystals of transition-metal Dichalcogenides, Phys. Rev. Lett. **113**, 077201 (2014).

[39] Y. Tang and A. E. Cohen, Optical chirality and its interaction with matter, Phys. Rev. Lett. **104**, 163901 (2010).

[40] B. Huang, G. Clark, E. Navarro-Moratalla, D. R. Klein, R. Cheng, K. L. Seyler, D. Zhong, E. Schmidgall, M. A. McGuire, D. H. Cobden *et al.*, Layer-dependent ferromagnetism in a van der Waals crystal down to the monolayer limit, Nature (London) **546**, 270 (2017).

[41] M. Gibertini, M. Koperski, A. F. Morpurgo, and K. S. Novoselov, Magnetic 2D materials and heterostructures, Nat. Nanotechnol. **14**, 408 (2019).

[42] N. Nagaosa, J. Sinova, S. Onoda, A. H. MacDonald, and N. P. Ong, Anomalous Hall effect, Rev. Mod. Phys. **82**, 1539 (2010).

[43] K. Swathi, C. Sissa, A. Painelli, and K. George Thomas, Supramolecular chirality: A caveat in assigning the handedness of chiral aggregates, Chem. Commun. **56**, 8281 (2020).

[44] B. Laidlaw, J. Eng, J. Wade, X. Shi, F. Salerno, M. J. Fuchter, and T. J. Penfold, On the factors influencing the chiroptical response of conjugated polymer thin films, Chem. Commun. **57**, 9914 (2021).

[45] G. Kresse and J. Furthmüller, Efficient iterative schemes for *ab initio* total-energy calculations using a plane-wave basis set, Phys. Rev. B **54**, 11169 (1996).

[46] J. P. Perdew, K. Burke, and M. Ernzerhof, Generalized gradient approximation made simple, Phys. Rev. Lett. **77**, 3865 (1996).

[47] A. A. Mostofi, J. R. Yates, Y.-S. Lee, I. Souza, D. Vanderbilt, and N. Marzari, wannier90: A tool for obtaining maximally-localised Wannier functions, Comput. Phys. Commun. **178**, 685 (2008).

[48] A. A. Mostofi, J. R. Yates, G. Pizzi, Y.-S. Lee, I. Souza, D. Vanderbilt, and N. Marzari, An updated version of wannier90: A tool for obtaining maximally-localised Wannier functions, Comput. Phys. Commun. **185**, 2309 (2014).

[49] G. Pizzi, V. Vitale, R. Arita, S. Blügel, F. Freimuth, G. Géranton, M. Gibertini, D. Gresch, C. Johnson, T. Koretsune *et al.*, Wannier90 as a community code: new features and applications, J. Phys.: Condens. Matter **32**, 165902 (2020).